Phys. Status Solidi A **214,** No. 10, 1700269 (2017) / **DOI** 10.1002/pssa.201700269

physica status solidi a
www.pss-a.com
applications and materials science

Tunable white light emission from hafnium oxide films co-doped with trivalent terbium and europium ions deposited by Pyrosol technique

J. C. Guzmán-Olguín[1], E. Montes[1], J. Guzmán-Mendoza[1], A. Báez-Rodríguez[2], L. Zamora-Peredo[2], M. García-Hipólito*[,3], O. Alvarez-Fregoso[3], I. Martínez-Merlín[4], and C. Falcony[4]

[1] Centro de Investigación en Ciencia Aplicada y Tecnología Avanzada del Instituto Politécnico Nacional, Unidad Legaria, Calzada Legaria 694. Colonia Irrigación, C.P. 11500, D.F, México
[2] Centro de Investigación en Micro y Nanotecnología, Universidad Veracruzana, Calzada Adolfo Ruiz Cortines 455, Fraccionamiento Costa Verde, 94292 Boca del Río, Ver México
[3] Instituto de Investigaciones en Materiales, Universidad Nacional Autónoma de México, Circuito Exterior, Ciudad Universitaria, Coyoacán, 04510, D.F, Mexico
[4] Centro de Investigación y de Estudios Avanzados del Instituto Politécnico Nacional, A.P. 14-740, 07360 D. F, México

Received 28 April 2017, revised 7 June 2017, accepted 8 June 2017
Published online 3 July 2017

Keywords HfO_2: Tb+Eu films, luminescence, Pyrosol, tunable emission, white light

* Corresponding autor: e-mail maga@unam.mx, Phone: +52 55 56 22 45 98, Fax:+52 55 5616 1361

In this paper, the photo and cathodoluminescent properties of HfO_2 films optically activated with different atomic concentrations of Tb^{3+} and Eu^{3+} ions, deposited by the Pyrosol technique, are reported. These films were deposited at temperatures from 400 to 600 °C, using chlorides as raw materials. The surface morphologies of all deposited films were rough and dense. X-ray diffraction analysis showed that the films deposited at 600 °C were polycrystalline exhibiting the HfO_2 monoclinic phase. The tuning by the means of the excitation wavelength generates photoluminescence spectra, for co-doped films, in several emissions from blue to yellow (including white light) due to the characteristic electronic transitions of Tb^{3+} (green), Eu^{3+}(red) ions and the violet-blue emission associated to the host lattice (HfO_2). According to the chromaticity diagram, the best white light is reached for the sample S2 excited with 382 nm ($x = 0.3343$, $y = 0.3406$). The cathodoluminescence emission spectra for co-doped films showed emissions from green to red (including yellow, orange and other intermediate emissions). The averaged quantum efficiency values of the sample labeled as S2 resulted between 47 and 78% depending on the excitation wavelength. In addition, XPS, TEM, SEM and decay times were performed to characterize these films.

1 Introduction The luminescent materials (phosphors) have played a key role in materials science, and they are required in a broad range of applications, which include: panel displays, scintillator devices, lasers, image projection radiography, fluorescent lamps, etc. Typically, the phosphors require a host lattice (generally a stable oxide) and an activator ion (rare earth or transition metal ion). Hafnium oxide (HfO_2) is regarded as a material technologically important because it exhibits high mechanical, thermal and chemical stabilities. The HfO_2 is a potential candidate to be used as a gas sensing, electrical insulator, in optoelectronic devices and anti-reflective optical coatings [1–5]. The HfO_2 films have a relatively high refractive index (1.89); this material has high optical transmission between 80 and 90% in the visible region and a near-infrared of the electromagnetic spectrum [6]. In addition, its high density and high effective atomic number makes it attractive as a scintillating material and due to its large band gap ($E_g = 5.68$ eV) and low phonon frequency (200–650 cm^{-1}), HfO_2 has been used as a host lattice for rare earth ions and transition elements in the production of luminescent materials [7–12]. The white light emitting phosphors are very important due to the large number of applications: in the outdoor, lighting with luminescent lamps increases the

visibility, thus reducing the number of accidents, while in the indoor lighting, the white luminescent lamps offer comfort and low power consumption. These applications require materials with high efficiency emitting in the three primary colors: blue, green and red, to generate white light emission [13–15]. Luminescent films, unlike those powdery materials, have the advantages such as excellent adhesion to the substrate, unchanged properties throughout the covered area, superior thermal stability, and negligible optical scattering with a smaller amount of material [16]. Currently, there are multiple and varied techniques for the films deposition, some of them are: Ion Beam Assisted Deposition [17], Pyrosol [18], Sputtering [19], Sol–Gel [20], Atomic Layer Deposition [21], etc. Among them, the Pyrosol process has proven to be a suitable technique to deposit thin, thick films and powdery materials; it is a simple and not expensive process that allows depositing films with different compositions, especially oxides. The precursor solutions used in the Pyrosol technique are derived from organic and inorganic salts such as chlorides, nitrates, acetates, acetylacetonates, etc., which are dissolved in deionized water, alcohols or other organic solvents. This deposition technique has some advantages such as low-priced, high rate deposition, operation easiness and the ability to deposit on substrates with relatively large areas [18]. Various investigations associated with the white light generation from metallic oxides host lattices activated with Eu^{3+} and Tb^{3+} ions can be found elsewhere [22–28]. To the best of our knowledge, there are very scarce reports on white light emitting films based on HfO_2 co-doped with $Eu^{3+} + Tb^{3+}$ ions.

This investigation reports on the synthesis and characterization photo and cathodoluminescent of hafnium oxide films co-doped with different concentrations of Tb^{3+} and Eu^{3+} ions, deposited by the Pyrosol technique; the purpose is to establish conditions (in the synthesis and optical excitation) to obtain white light emission, using only two activator ions such as Tb^{3+} (green), Eu^{3+} (red) and the intrinsic (violet-blue) host lattice emission.

2 Experimental A 0.08 M precursor solution of hafnium chloride ($HfCl_4$) (Alfa-Aesar, 99.9% purity) dissolved in deionized water was used to deposit un-doped hafnium oxide films. These films were deposited on Corning 7059 glass (for XRD, SEM and luminescence measurements) and on silicon single-crystals substrates (for XPS measurements) at temperatures of 400, 450, 500, 550, and 600 °C; in all cases the deposition times were 6 min and the carrier gas flow (dry and filtered air) was 10 liter min^{-1}. HfO_2:Eu^{3+} and HfO_2:Tb^{3+} films were deposited as a function of the doping concentrations; it was determined that the relative concentrations of 10 at.% for Eu^{3+} ions and 5 at.% for Tb^{3+} ions were the best luminescent doping conditions. In addition, these films were deposited as a function of the substrate temperature; it was observed that films deposited at 600 °C showed the highest emission intensity. Co-doped films (with Tb^{3+} and Eu^{3+} ions) were deposited from different combinations of two precursor solutions (solution A and solution B). Solution A was prepared by dissolving 0.08 M of ($HfCl_4$) in deionized water and doped with europium chloride hexahydrate ($EuCl_3.6H_2O$, Sigma Aldrich Chemical Co., 99.99% purity), the europium concentration was 10 at.% with respect to Hf content. Solution B was prepared similarly to solution A; in this case the doping was reached with terbium chloride hexahydrate ($TbCl_3.6H_2O$, Sigma–Aldrich Chemical Co., 99.99% purity), here the terbium concentration was 5 at.%. Subsequently, these solutions (A and B) were combined in volume (up to 100 ml) to yield seven different solutions, each one with different percentages of the activator ions (these solutions were labeled as: S1, S2 ... S7). The different combinations of solutions A and B are shown in the Table 1. For example, solution S1 is constituted by 0 ml of solution A + 100 ml of solution B; solution S2 is formed by 20 ml of solution A + 80 ml of solution B; and so on. These solutions were used to deposit the films studied in this investigation. The samples labeled as Sn ($n = 1, 2, 3, \ldots 7$) were synthesized from solutions Sn. In all cases the substrate temperature was 600 °C. The deposited films were characterized by X-Ray Diffraction (XRD) with a D-5000 SIEMENS diffractometer using a wavelength of 1.5406 Å, corresponding to the Kα emission line of the copper ($Cu_{K\alpha}$). The surface morphology was analyzed by Scanning Electron Microscopy (SEM) in a Cambridge-Leica, Stereoscan 440 microscope. High resolution transmission electron microscopy (HRTEM) was performed by means of a JEOL microscope model JEM-ARM 200 CF. The chemical composition inside the films was measured by X-ray Photoelectron Spectroscopy; XPS analyses were performed in an UHV system Scanning XPS microprobe PHI 5000 VersaProbe II, with a Al Kα X-ray source ($h\nu = 1486.6$ eV) monochromatic and a MCD analyzer. The XPS spectra were obtained at 45° to the normal surface in the constant pass energy mode (CAE), $E_0 = 117.40$ for survey surface. The photoluminescence (PL), excitation and emission spectra and delay times were obtained at room temperature, using an Edinburgh

Table 1 Precursor solutions used in the deposition of co-doped hafnium oxide films with europium and terbium ions.

deposition solutions		
sample	solution A (Eu^{3+}:10 at.%), ml	solution B (Tb^{3+}:5 at.%), ml
S1	0	100
S2	20	80
S3	40	60
S4	50	50
S5	60	40
S6	80	20
S7	100	0

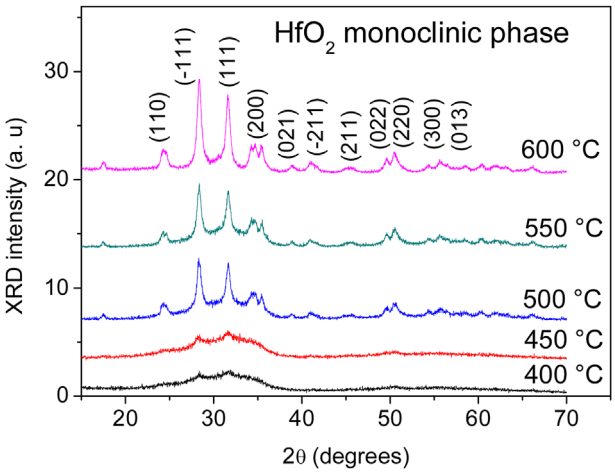

Figure 1 XRD diffractograms of HfO_2 films deposited at different deposition temperatures.

Instruments fluorescence spectrometer model FLS980 equipped with an integration sphere to quantum yield (QY) measurements. The Cathodoluminescence (CL) measurements were carried out in a Luminoscope model ELM-2MCA, RELION Co, which consists of a stainless steel vacuum chamber equipped with a cold cathode electron gun attached to the above-mentioned spectrometer by an optical fiber bundle. The thickness of the films was approximately 6 μm as measured by a Sloan Dektak IIA profilometer. Finally, the color corresponding to the luminescent emission of the films was evaluated by the means of the CIE coordinates in the chromaticity diagrams.

3 Results and discussion Figure 1 shows the results of analyses by XRD carried out on the HfO_2 films at different deposition temperatures. The diffraction patterns of the films deposited at temperatures below 450 °C do not exhibit well-defined peaks, indicating that these films remain mainly amorphous. However, the diffractograms of the films deposited at substrate temperatures higher than 450 °C, show a polycrystalline structure with diffraction peaks corresponding to the HfO_2 monoclinic phase (431017 JCPDS card). The peaks have been indexed in the figure, where it is possible to see a (−111) preferential orientation. The crystal size of the particles that constitute the film deposited at 600 °C, was estimated from the two stronger reflections (−111) and (111) using the Scherrer formula, the averaged crystal size was 15 nm.

The chemical composition was determinated by X-ray photoelectron spectroscopy. Table 2 shows the chemical composition measurements obtained by XPS for co-doped HfO_2 films (deposited at 600 °C) with different proportions of terbium and europium ions. This table shows relative atomic percentages of oxygen, hafnium, europium, terbium and carbon inside the layers, as a function of the percentages of the precursor solutions used. From these XPS measurements it is possible to observe that the obtained values for oxygen are not far from the ideal theoretical value, yielding an average value for these samples of 65.62 at.%. Furthermore, hafnium also maintains acceptable behavior, the average value was 31.02 at.%, very close to the ideal stoichiometry of hafnium oxide. Also, an amount of carbon in all samples was observed, reaching values around 1–2 at.%. In addition, different quantities of Terbium and Europium ions (1–2 at.%) were observed. The sample labeled as S0 is that without rare earths ions doping. The corresponding XPS spectra of four HfO_2 samples are shown in Fig. 2. Here, it is possible to observe typical XPS wide survey spectra of samples S0 (a), S7 (b), S1 (c) and S2 (d). These spectra show peaks belonging to: Hf (Hf 4f at 18 eV; Hf 4d at 213 eV and Hf 4p at 380), O (O 1s at 530 eV and O_{KLL} at 976 eV), Eu (Eu 3d at 1124 and 1156 eV), Tb (Tb 3d at 1242 and 1274 eV) and C (C 1s at 285 eV). The detected C is related to the carbon adsorbed on the surface during the exposure of the films to the ambient atmosphere [29]. The Hf $4f_{7/2}$ peak at $E = 18$ eV indicates the formation of Hf–O bonding and Hf^{4+} oxidation number within the HfO_2 films, this is in good agreement with the reported literature [30].

Figure 3 shows SEM micrographs of the surface morphology for three HfO_2 films deposited at 600 °C: a) un-doped sample; b) co-doped (sample S2), c) co-doped (sample S6), and d) a cross section of the un-doped sample. In all of them, it is possible to observe continuous films with rough surfaces, which can be an advantage for some applications due to the large surface area provided by these films. The surface microstructure of the un-doped layers (Fig. 2a) exhibits clusters of spherical particles, which cover the entire surface of the substrate. These spherical particles are approximately 2 μm in diameter. The microstructure of

Table 2 Relative atomic percentages of the elements present inside the HfO_2: $Eu^{+3} + Tb^{+3}$ films, as measured by X-ray Photoelectron spectroscopy (XPS).

	co-doped samples deposited at 600 °C							
element (at.%)	S0	S1	S2	S3	S4	S5	S6	S7
oxygen	67.29	67.92	65.43	64.87	65.58	65.86	64.95	65.83
carbon	1.77	1.24	1.25	1.15	1.39	1.84	1.81	1.69
hafnium	30.94	30.84	33.32	33.98	33.03	32.30	33.24	32.48
terbium	0.0	1.51	1.35	1.16	1.08	0.84	0.66	0.0
europium	0.0	0.0	0.88	1.13	1.26	1.48	1.96	2.15

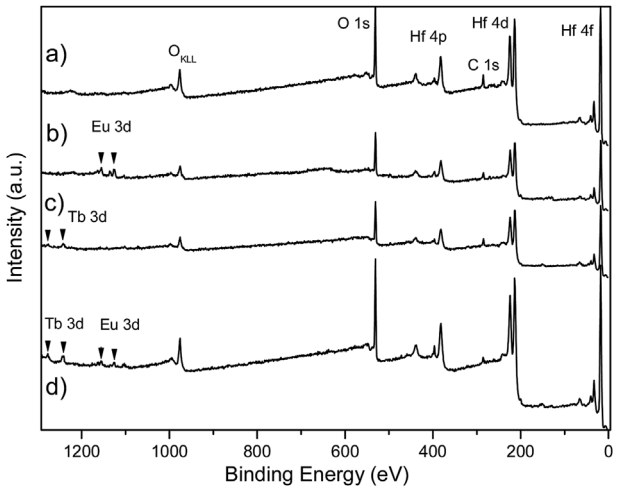

Figure 2 XPS survey spectra of samples: S0 (a), S7 (b), S1 (c), and S2 (d).

the co-doped films, sample S2, with high Tb^{3+}ions content (Fig. 2b) clearly show the formation of island of spherical particles as well as a branch shaped microstructure. The microstructure of the co-doped films, with high Eu^{3+}ions content, sample S6, (Fig. 2c) shows an intermediate state between un-doped films and the co-doped films with high Tb^{3+} ions content. In general, some changes on the surface microstructure of the co-doped layers are observed with the incorporation of rare earths ions (Eu^{3+} and Tb^{3+}). Fig. 2d) shows a cross section of the un-doped sample; here it is possible to observe that the films are formed by a solid base of approximately 2 μm and on this base clusters or heaps of spherical particles; as a consequence the films exhibit high roughness.

A high resolution transmission electron microscopy image (HRTEM), taken in HfO_2 films deposited on Si substrate at 600 °C, is observed in Fig. 4. This polycrystalline film consists of nanograins, which exhibit atomic fringes corresponding to low index lattice planes of hafnium oxide structure. The HfO_2 grains have an irregular morphology with diameters ranging from 5 to 15 nm. These values coincide approximately with those estimated by the Scherrer formula.

Figure 5a shows PL emission spectrum of HfO_2 films doped with Tb^{3+} ions, which were synthesized at 600 °C and excited with 266 nm. The bands centered at 490, 543, 590, and 623 nm, correspond to transitions from the excited state $^5D_4$ toward $^7F_6$, $^7F_5$, $^7F_4$ and $^7F_3$ levels, respectively; the most intense band is centered at 543 nm. Figure 5b exhibits the PL excitation spectrum of the same HfO_2:Tb^{3+} films, which was monitored with an emission wavelength at 543 nm. Here, it is possible to observe a spectrum with a broad band from 240 to 310 nm centered at 266 nm, which is attributed to the $4f^8$–$4f^75d^1$ transition of Tb^{3+} ions, and the small peaks with the position from 320 to 400 nm belong to the transitions between energy levels of the $4f^8$ configuration of Tb^{3+}ions [31, 32]. Figure 5c shows the dependence of the emission intensity of the band centered at 543 nm for HfO_2:Tb^{3+} films as a function of the doping concentration; these films were deposited at 600 °C and excited with a wavelength of 266 nm; such emission intensity increases depending on the concentration of Tb^{3+} ions, which reach its maximum emission intensity for 5 at.%; at higher concentrations than 5 at.%, the emission intensity decreases, very probably due to the concentration quenching phenomena.

Figure 6a shows the photoluminescence emission spectrum for HfO_2:Eu^{3+} films, deposited at 600 °C and

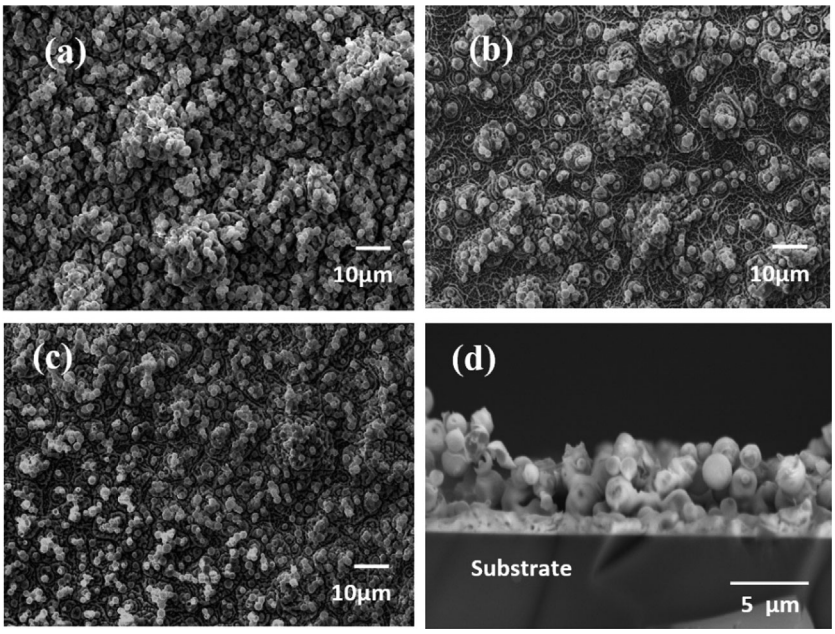

Figure 3 SEM Micrographs of three different HfO_2 films deposited at 600 °C; a) un-doped sample; b) co-doped sample S2; c) co-doped sample S6 and d) cross section view of the un-doped sample.

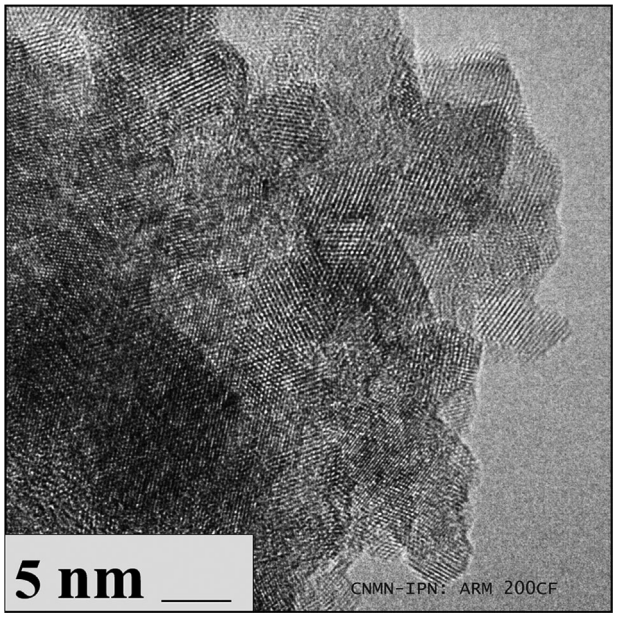

Figure 4 High resolution transmission electron microscopy image (HRTEM) from HfO_2 films deposited on Si substrate at 600 °C.

excited with 262 nm. Typical emissions of Eu^{3+} ions are observed and located at 578, 592, 613, 654, and 703 nm, which correspond to transitions: $^5D_0 \rightarrow {}^7F_0$, $^5D_0 \rightarrow {}^7F_1$, $^5D_0 \rightarrow {}^7F_2$, $^5D_0 \rightarrow {}^7F_3$, and $^5D_0 \rightarrow {}^7F_4$, respectively; the most intense band is located at 613 nm. Figure 6b exhibits the excitation spectrum of HfO_2:Eu^{3+} films, synthesized at 600 °C and monitored at 613 nm, in which a broad band centered at 262 nm is the most intense, this band is attributed to a charge transfer from the p orbitals of the O^{2-} ions to f orbitals of Eu^{3+} ions. Also, the typical absorption bands of the Eu^{3+} ions can be observed, which are located at 361, 380, 395, 414, and 466 nm, these correspond to the electronic transitions from the ground state $^7F_0$ to the excited states $^5D_4$, $^5G_4$, $^5L_6$, $^5D_3$, and $^5D_4$, respectively [6]. The dependence of the PL emission intensity of the HfO_2:

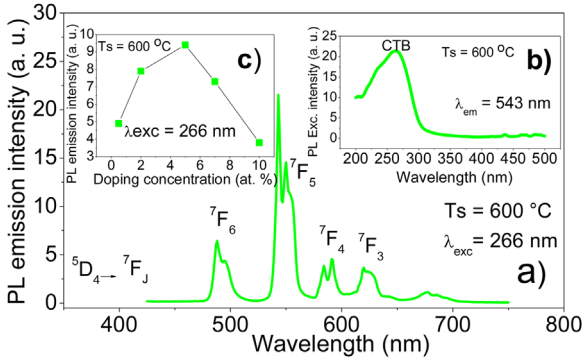

Figure 5 a) PL Emission spectrum of HfO_2: Tb^{3+} films synthesized at 600 °C. b) Excitation spectrum of HfO_2: Tb^{3+} films synthesized at 600 °C. c) Emission intensity dependence of HfO_2: Tb^{3+} films as a function of the doping concentration.

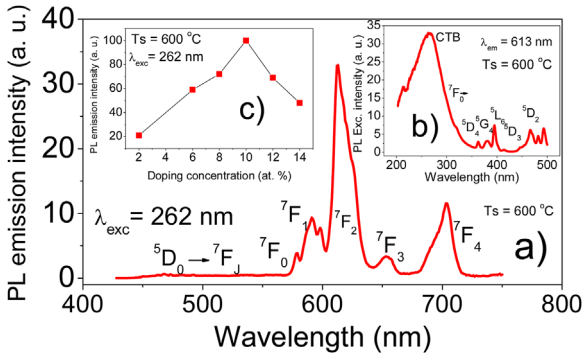

Figure 6 a) PL Emission spectrum of HfO_2: Eu^{3+} films deposited at 600 °C. b) Excitation spectrum of HfO_2: Eu^{3+} films synthesized at 600 °C. c) Behavior in PL emission intensity of HfO_2: Eu^{3+} films depending on the doping concentration.

Eu^{3+} films (intensities of the band centered at 613 nm) as a function of the doping concentration is shown in Fig. 6c; synthesis of these films was carried out at 600 °C and excited with 262 nm. It is observed that the PL emission intensity increases when the Eu^{3+} ions concentration is raised. The maximum emission intensity is reached for 10 at.% of Eu^{3+} ions (in the start solution), after this value the PL emission intensity decreases, surely due to the quenching concentration effect.

Three PL excitation spectra for the sample deposited from the solution labeled as S2 are displayed in Fig. 7. This film shows the best luminescent characteristics to reach the white light emission. Curve (a) corresponds to host lattice as monitored at 420 nm; curve (b) is associated to Tb^{3+} ions as monitored at 543 nm and curve (c) is for Eu^{3+} ions as monitored at 613 nm. In this case, it is possible to observe that the excitation spectra for Eu^{3+} and Tb^{3+} ions show

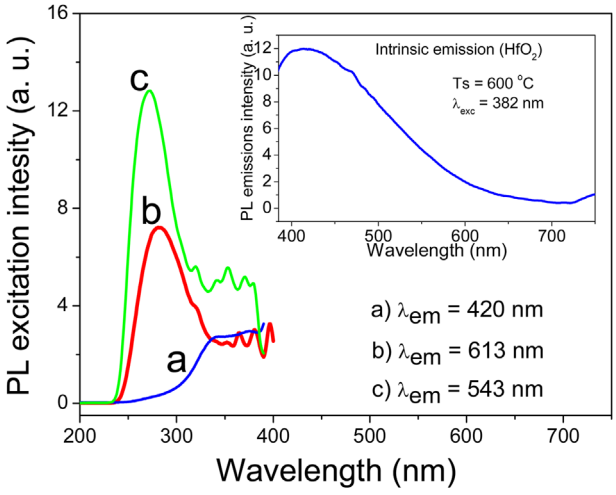

Figure 7 Excitation spectra of the layer S2, exciting the host lattice ($\lambda_{em} = 420$ nm), exciting the Eu^{3+} ions ($\lambda_{em} = 613$ nm) and exciting the Tb^{3+} ions ($\lambda_{em} = 543$ nm), synthesized at 600 °C. The inset shows the emission spectrum for the un-doped sample ($\lambda_{ex} = 382$ nm).

prominent and broad bands centered approximately at 271 and 282 nm, respectively; these bands are similar to those showed in Figs. 5b and 6b, even though the presence of both impurities ($Eu^{3+} + Tb^{3+}$ ions) into the host lattice causes some small differences in the excitation spectra. In addition, the host lattice (HfO_2) exhibits an irregular broad band in the region from 300 to 400 nm. From these spectra, it is possible to see that Eu^{3+} and Tb^{3+} ions can be excited with wavelengths from 235 to 400 nm while the host lattice is excited only in the region from 300 to 400 nm. This suggests that the excitation with wavelengths from 300 to 400 nm could simultaneously excite the three primary colors: red (from Eu^{3+} ions), green (from Tb^{3+} ions) and blue (from host lattice) to generate white light. Inset of the Fig. 7 shows the PL emission spectrum for un-doped HfO_2 films; the excitation wavelength was 382 nm. In this case, a broad band is observed; this band exhibits a maximum at about 420 nm (violet-blue region). It has been reported that HfO_2 emits violet-blue light, which is attributed to defects such as oxygen deficiencies [33, 34].

In Fig. 8 the PL emission spectra of the films referred to as S1 to S7 can be observed, which contain different ratios of Tb^{3+}/Eu^{3+} according to Table 1. These samples were synthesized at 600 °C and excited with 382 nm (see Fig. 11). The emission spectrum of the sample S1 (which only contains Tb^{3+} ions) shows the typical PL emissions for Tb^{3+} ions, and the most intense band is centered at 547 nm. In addition, a wide band between 400 and 480 nm is observed, centered about 425 nm, which can be attributed to the host lattice emissions. In the sample labeled as S7, which contains only Eu^{3+} ions, the PL emission spectrum shows the own emission of Eu^{3+} ions and also the emission of the host lattice can be observed, with lower intensity than for sample S1. The PL emission spectrum of sample S2, maintains a more balanced relationship in the intensities of the major bands of Tb^{3+} and Eu^{3+} ions. Nevertheless, the band corresponding to the main emission of Tb^{3+} ions is more intense, and centered 547 nm. In this spectrum, the host lattice emission is less intense than for all other spectra. The above is reversed for the spectrum of sample S3, because now the most intense band is centered at 615 nm, which corresponds to the transition $^5D_0 \rightarrow {}^7F_2$ of Eu^{3+} ions. It continues to increase in intensity until sample S7, while the band centered at 547 nm, corresponding to the transition $^5D_4 \rightarrow {}^7F_5$ of the Tb^{3+} ions, decreases.

Figure 9 shows the CIE chromaticity diagram for PL emission spectra presented in Fig. 8. The chromaticity coordinates corresponding to each point on the CIE diagram can be seen in the inserted table. The sample labeled as S1, has chromaticity coordinates (0.2201, 0.2548) corresponding to blue-green emission, this sample contains only terbium ions, and the notable blue contribution comes from the host lattice emission. Sample S2 shows white emission with chromaticity coordinates (0.3350, 0.3423), which are very close to perfect white emission. All other samples showed points, in chromaticity diagram, corresponding to reddish emissions.

PL emission spectra for HfO_2:$Tb^{3+} + Eu^{3+}$samples labeled as S2 are shown in Fig. 10, which were obtained by varying the excitation wavelength from 366 to 390 nm, in order to achieve the best tuning of three basic colors to produce a white emission. All spectra are similar, except for the broad band in 400–450 nm region. This broad band is attributed to emission from the host lattice, as mentioned above, which becomes more intense as the excitation wavelength increases.

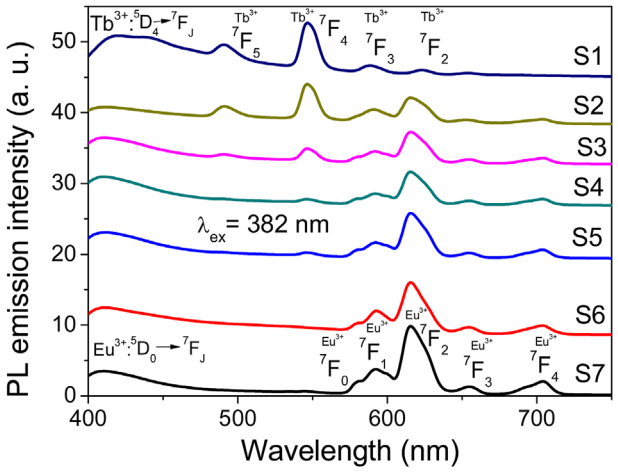

Figure 8 PL emission spectra for HfO_2: $Tb^{3+} + Eu^{3+}$ films with different contents of Tb^{3+} and Eu^{3+} ions; synthesized at 600 °C.

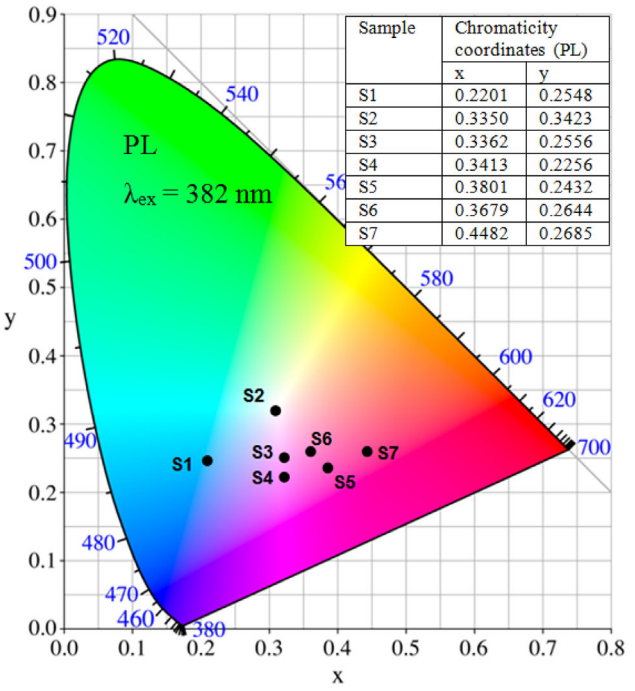

Sample	Chromaticity coordinates (PL)	
	x	y
S1	0.2201	0.2548
S2	0.3350	0.3423
S3	0.3362	0.2556
S4	0.3413	0.2256
S5	0.3801	0.2432
S6	0.3679	0.2644
S7	0.4482	0.2685

Figure 9 CIE Chromaticity Diagram for PL emission spectra of HfO_2:$Tb^{3+} + Eu^{3+}$ films with different contents of the Tb^{3+} and Eu^{3+} ions, $\lambda_{ex} = 382$ nm.

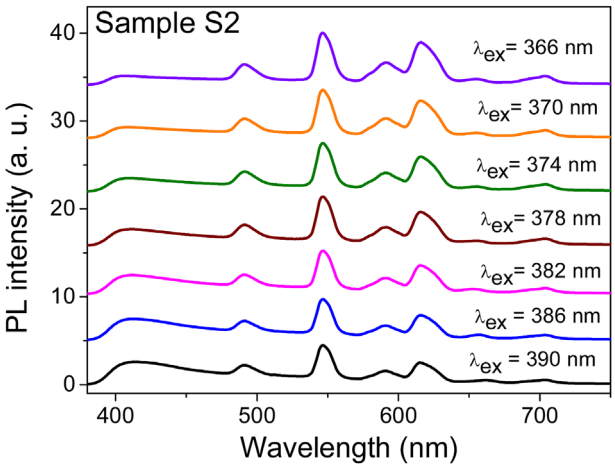

Figure 10 PL emission spectra for the sample S2 as a function of the excitation wavelength.

Figure 11 shows CIE chromaticity diagram for PL spectra of sample S2 (Fig. 10). The CIE coordinates are represented by points labeled as a, b, c, d, e, f, and g, corresponding to the wavelength with which they were excited, 366, 370, 374, 378, 382, and 386 nm, respectively. The chromaticity diagram exhibits that as this sample was excited from 366 until 386 nm, different emissions were obtained from warm white to cold white. First, exciting with 366 nm, a yellow emission or warm white was obtained. As the excitation wavelength was increased, the color was approaching to the perfect white (0.3333, 0.3333) through

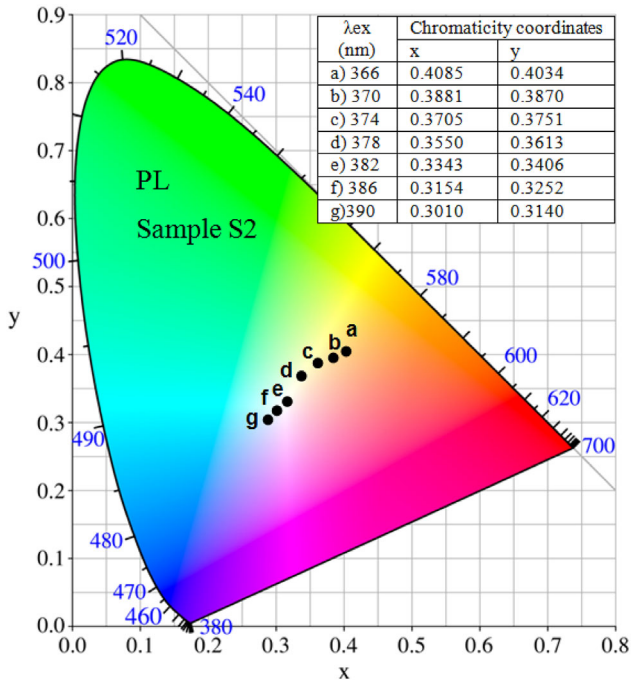

Figure 11 CIE chromaticity diagram for sample S2 as a function of the excitation wavelength.

different tones of yellow, until the excitation wavelength of 382 nm where the sample emits a white light (very close to ideal), with chromaticity coordinates (0.3343, 0.3406). In this case, de Color Temperature was 5385 K as calculated by the McCamy formula [35]. If the excitation wavelength increases, the host lattice is better excited, such that now blue or cold white emission is obtained (points: f and g). As a consequence, 382 nm wavelength was selected to excite the co-doped samples with different Tb/Eu ratios.

CL emission spectra for the series of HfO_2:Tb^{3+} + Eu^{3+} samples with different concentrations of Tb^{3+} and Eu^{3+} ions, according to Table 1, are presented in Fig. 12. The sample labeled as S1exhibits, as in the PL emissions, the typical emissions of Tb^{3+} ions; in the same way the sample labeled as S7 shows typical emissions from Eu^{3+} ions. In the sample S6 the band centered at 547 nm (Tb^{3+} ion transition) appears with very low intensity which is enhanced as the content of Tb^{3+} ions is increased in the other samples, while the emission at 615 nm (Eu^{3+} ion transition) decreases. A notable difference with respect to the PL emission spectra is observed; since none of the spectra of this figure show the violet-blue broad band attributed to HfO_2 host lattice. More investigation is in course to elucidate this point.

The CIE chromaticity diagram for CL emission spectra of the HfO_2:Tb^{3+} + Eu^{3+}samples with different concentrations of Tb^{3+} and Eu^{3+} ions is presented in Fig. 13. In the table (inset) the corresponding chromaticity coordinates can be observed. It is clear that sample S7, which only has Eu^{3+} ions, shows a red emission purer than other samples, and as Tb^{3+} ions are incorporated there is a trend approaching to yellow emissions; therefore, the samples labeled as S6, S5, S4 exhibited red-orange emissions, but the sample S3 indicates a yellow emission due to the higher Tb^{3+} ions content. The sample labeled as S2 shows a yellow-green emission, while sample S1 exhibits a green emission typical of Tb^{3+} ions. Finally, is possible to mention that all

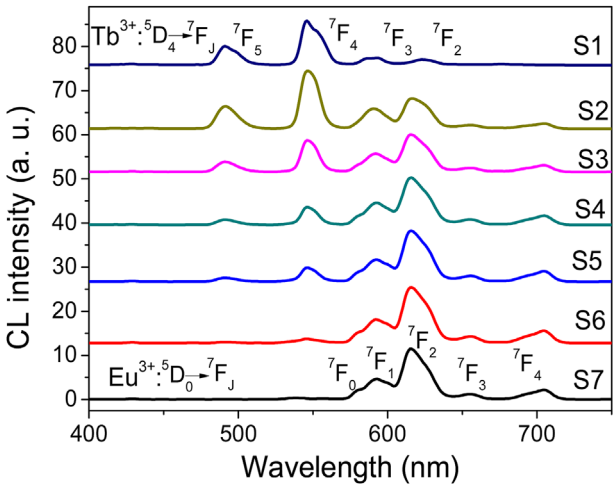

Figure 12 CL emission spectra for HfO_2:Tb^{3+} + Eu^{3+} films as a function of the different contents of Tb^{3+} and Eu^{3+} ions; synthesized at 600 °C.

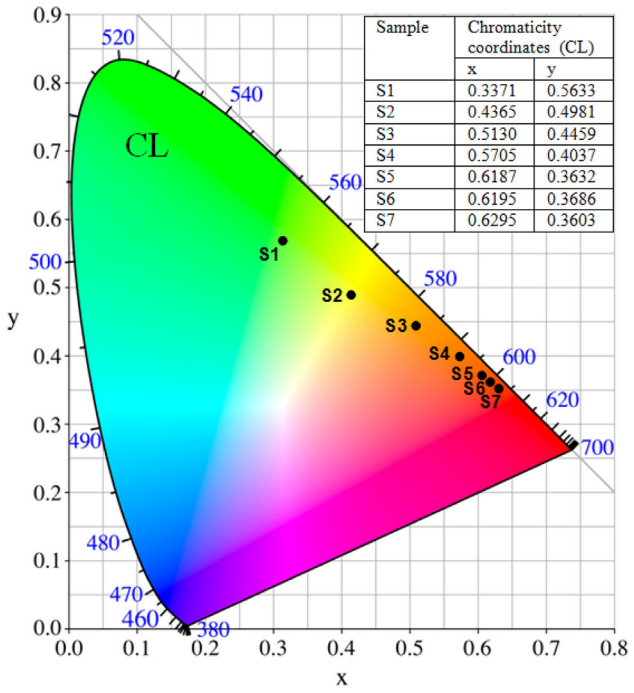

Sample	Chromaticity coordinates (CL)	
	x	y
S1	0.3371	0.5633
S2	0.4365	0.4981
S3	0.5130	0.4459
S4	0.5705	0.4037
S5	0.6187	0.3632
S6	0.6195	0.3686
S7	0.6295	0.3603

Figure 13 CIE Chromaticity diagram for CL emission spectra of the HfO_2:Tb^{3+} + Eu^{3+} films with different amounts of Tb^{3+} and Eu^{3+} ions.

the emissions obtained by CL are between red and green because the host lattice was not excited by the accelerated electrons.

Life-time measurements of sample S2 were performed by excitation with 382 nm monitoring the emissions at 420, 543, and 613 nm. Figure 14 shows the decay profiles

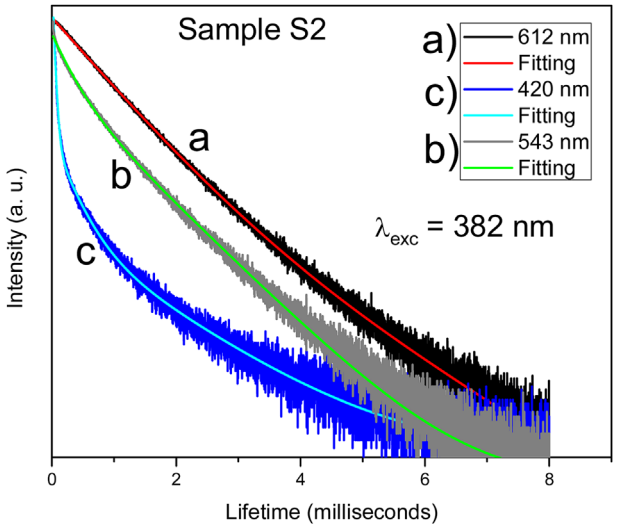

Figure 14 Life-time measurements of sample S2 performed by excitation with 382 nm monitoring the emissions at 420, 543, and 613 nm.

associated with Tb^{3+} ions (543 nm), Eu^{3+} ions (613 nm) and HfO_2 (420 nm) of sample S2.

The decay curves for transitions of Tb^{3+} ions and Eu^{3+} ions were fitted with a double-exponential function as

$$I = A + B_1\exp(-t/\tau_1) + B_2\exp(-t/\tau_2),$$

here, I is the intensity and A (background), B_1, B_2, and τ_1, τ_2 are the fitting parameters. The decay curve for the transition of the host lattice (HfO_2) at 420 nm was fitted with a triple-exponential function as

$$I = A + B_1\exp(-t/\tau_1) + B_2\exp(-t/\tau_2) + B_3\exp(-t/\tau_3),$$

where once again, I is the intensity and A (background), B_1, B_2, B_3 and τ_1, τ_2, τ_3 are the fitting parameters [6]. The average decay times, τ_{av}, were calculated using these parameters and the following equation:

$$\tau_{av} = \left[\Sigma B_i(\tau_i)^2\right]/[\Sigma B_i(\tau_i)].$$

The average decay times calculated from these fits were 0.97, 1.23, and 0.57 ms for Tb^{3+} ions, Eu^{3+} ions, and HfO_2, respectively. The average decay times for Tb^{3+} and Eu^{3+} ions are similar to those obtained in other investigations [6, 36].

Photographs on HfO_2:Tb^{3+} + Eu^{3+}samples can be seen in Fig. 15. Photograph a) shows the samples labeled as S1 to S7, which were excited by a wavelength of 254 nm provided by a UV lamp. Mainly green, yellow, orange and red

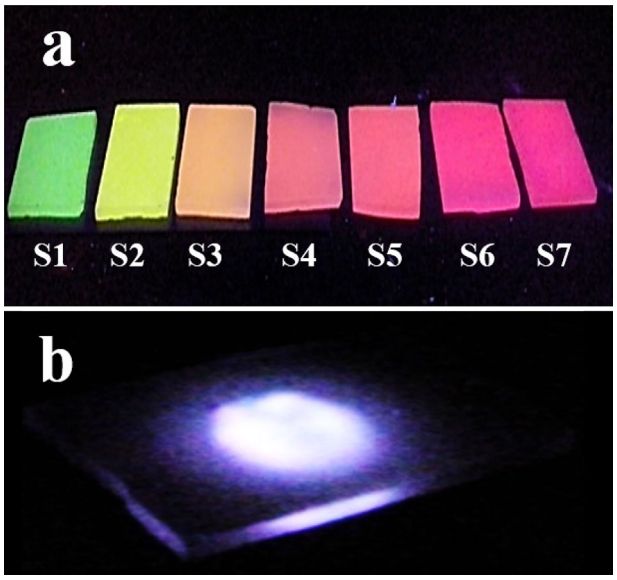

Figure 15 Photographs of a) HfO_2:Tb^{3+} + Eu^{3+} films labeled S1, S2, S3, S4, S5, S6, and S7, excited with 254 nm provided by a UV lamp; b) HfO_2:Tb^{3+} + Eu^{3+} film S2, excited with 382 nm provided by the fluorescence spectrometer.

emissions are observed because the excitation wavelength (254 nm) does not excite significantly to the host lattice (HfO_2), therefore the violet-blue contribution is not observed. Picture b) shows the white light emission from a co-doped HfO_2: $Tb^{3+} + Eu^{3+}$sample labeled as S2, which was excited with 382 nm provided by the fluorescence spectrometer cited in the experimental details.

PL absolute quantum efficiency (QE) of the sample labeled as S2 was measured (five times); the averaged value obtained was 47%, when it was excited with 382 nm and 78% if the sample is excited with 280 nm. The QE values were calculated by the following equation [37]:

$$\eta(\mathrm{QE}) = \frac{\int L_{\mathrm{emission}}}{\int E_{\mathrm{blanc}} - \int E_{\mathrm{sample}}}$$

where L_{emission} is the emission spectrum of the studied sample, E_{sample} is the spectrum of the light used for exciting the sample and E_{blanc} is the spectrum of the excitation light without the sample in the integration sphere. The values obtained in this material (HfO_2: $Tb^{3+} + Eu^{3+}$) for quantum efficiency are high and are suitable for various applications, for example in white LEDs excited with near UV radiation [37]:

4 Conclusions In this contribution, un-doped (HfO_2) and co-doped (HfO_2: $Tb^{3+} + Eu^{3+}$) films were successfully synthesized by the means of Pyrosol process. The deposition temperature was an important parameter to improve the crystalline structure of these layers; at low temperature (400–450 °C) these films were non-crystalline, while films deposited at higher temperatures (500–600 °C) showed the polycrystalline structure of the HfO_2 monoclinic phase. The best quality of crystalline structure was reached at 600 °C, this substrate temperature is relatively low compared to those used in the synthesis of powdery samples. The crystal size of the layers deposited at 600 °C was about 5–15 nm (as measured by HRTEM), which are similar to those estimated by the Scherrer formula. The SEM micrographs showed that the films deposited at highest substrate temperature are continuous and rough, crowned by clusters of spherical particles; these characteristics allow to the luminescent layers have a greater interaction surface area with the excitation radiation. The chemical composition was determinated by XPS, and it was observed that the ratio Hf/O is close to the ideal stoichiometry of the HfO_2. In addition, the delay times of the sample S2 were obtained, and the average delay times for Tb^{3+} and Eu^{3+} ions are similar to those reported in other investigations. Also, quantum efficiency (QE) of the sample labeled as S2 was measured; the averaged value obtained was 47%, when excited with 382 nm, and 78%, if the sample is excited with 280 nm. The quantum efficiency values for the studied material in this research are considerably high and are appropriate for many applications, such as white LEDs excited with near UV radiation. The methodology used in the preparation of the precursor solutions allowed to synthesize films activated with different concentrations of trivalent Tb^{3+} and Eu^{3+} ions; these samples exhibited a strong intensity photo and cathodoluminescent and various emissions ("colors") could be easily obtained by tuning the excitation wavelength and the ratio Tb^{3+}/Eu^{3+}. As a consequence, red, orange, yellow, green, violet-blue, and notably, white light emissions were generated using only two activators (Tb^{3+} and Eu^{3+}). The white light obtained from sample S2 excited with 382 nm, could be proposed for lighting devices excited with laser diodes (LEDs), now commercially available (360–410 nm); therefore, this material shows a great advantage because it avoids the use of mercury lamps as an excitation source.

Acknowledgements The authors would like to thank to Adriana Tejeda, L. Huerta, M. Guerrero, Z. Rivera, C. Flores and R. Reyes for their technical support; also, to CONACYT México and SIP-IPN for the financial support through the project 20150189.

References

[1] S. Capone, G. Leo, R. Rella, P. Siciliano, and L. Vasanelli, J. Vac. Sci. Technol. A **16**, 3564–3568 (1998).
[2] A. Avila-García and M. García-Hipólito, Sens. Actuators B **133**, 302–307 (2008).
[3] J. Domaradzki, D. Kaczmarek, E. L. Prociow, A. Borkowska, R. Kudrawiec, J. Misiewicz, D. Schmeisser, and G. Beuckert, Surf. Coat. Technol. **200**, 6283–6287 (2006).
[4] S. M. Edlou, A. Smajkiewicz, and G. A. Al-Jumaily, Appl. Opt. **32**, 5601–5605 (1993).
[5] J. M. Khoshman, A. Khan, and M. E. Kordesch, Surf. Coat. Technol. **202**, 2500–2502 (2008).
[6] I. Martínez-Merlín, J. Guzmán-Mendoza, M. García-Hipólito, V. M. Sánchez-Resendiz, L. Lartundo-Rojas, R. J. Fragoso, and C. Falcony, Ceram. Int. **42**, 2446–2455 (2016).
[7] V. Kiisk, I. Sildos, S. Lange, V. Reedo, T. Tatte, M. Kirm, and J. Aarik, Appl. Surf. Sci. **247**, 412–417 (2005).
[8] M. Villanueva-Ibañez, C. Le luyer, C. Dujardin, and J. Mugnier, Mater. Sci. Eng. B **105**, 12–15 (2003).
[9] M. García-Hipólito, O. Alvarez-Fregoso, J. Guzmán, E. Martínez, and C. Falcony, Phys. Status Solidi A **201**, R127–R130 (2004).
[10] C. Chacón-Roa, J. Guzmán-Mendoza, M. Aguilar-Frutis, M. García-Hipólito, O. Alvarez-Fragoso, and C. Falcony, J. Phys. D: Appl. Phys. **41**, 015104–(7pp) (2008).
[11] D. A. Neumayer and E. Cartier, J. Appl. Phys. **90**, 1801–1808 (2001).
[12] X. Zhao and D. Vanderbilt, Phys. Rev. B **65**, 233106 (2002).
[13] R.-J. Xie and N. Hirosaki, Sci.Technol. Adv. Mater. **8**, 588–600 (2007).
[14] C. R. Ronda, J. Lumin. **72–74**, 49–54 (1997).
[15] L. Liu, Y. Wang, Y. Su, Z. Ma, Y. Xie, H. Zhao, C. Chen, Z. Zhang, and E. Xie, J. Am. Ceram. Soc. **94**, 2141–2145 (2011).
[16] G. A. Hirata, J. McKittrick, M. Avalos-Borja, J. M. Siqueiros, and D. Devlin, Appl. Surf. Sci. **113/114**, 509–514 (1997).

[17] T. Mori, M. Fujiwara, R. R. Manory, I. Shimizu, T. Tanaka, and S. Miyake, Surf. Coat. Technol. **169-170**, 528–531 (2003).
[18] M. Langlet and J. Joubert, The pyrosol process or the pyrolysis of an ultrasonically generated aerosol, Chemistry of Advanced Materials, edited by C. N. R. Rao, (Blackwell, Oxford, 1993), p. 55.
[19] L. Pereira, A. Marques, H. Águas, N. Nedev, S. Georgiev, E. Fortunato, and R. Martins, Mater. Sci. Eng. B **109**, 89–93 (2004).
[20] Z. J. Wang, T. Kumagay, H. Kokawa, J. Tsuaur, M. Ichiki, and R. Maeda, J. Cryst. Growth **281**, 452–457 (2005).
[21] G. Scarel, S. Spiga, C. Wiemer, G. Tallarida, S. Ferrari, and M. Fanciulli, Mater. Sci. Eng. B **109**, 11–16 (2004).
[22] V. H. Romero, E. De la Rosa, T. López-Luke, P. Salas, and C. Angeles-Chavez, J. Phys. D: Appl. Phys. **43**, 465105–(8pp) (2010).
[23] H. Miao, R. Ji, X. Hu, L. Han, Y. Hao, Q. Sun, D. Zhang, J. Fan, J. Bai, and X. Hou, J. Alloy. Compd. **629**, 74–79 (2015).
[24] S. Mukherjee, D. P. Dutta, N. Manoj, and A. K. Tyagi, J. Nanopart. Res. **14**, 814–(10pp) (2012).
[25] E. Álvarez, Ma. E. Zayas, J. Alvarado-Rivera, F. Félix-Domínguez, R. P. Duarte-Zamorano, and U. Caldiño, J. Lumin. **153**, 198–202 (2014).
[26] G. Bai, M. K. Tsang, and J. Hao, Adv. Opt. Mater. **3**, 431–462 (2015).
[27] G. Bai, M. K. Tsang, and J. Hao, Adv. Funct. Mater. **26**, 6330–6350 (2016).
[28] L. Cheng, M. C. Wang, G. Bai, W. Jie, and J. Hao, Nano Energy **14**, 372 (2015).
[29] R. Al-Gaashania, S. Radiman, A. R. Daud, N. Tabet, and Y. Al-Douri, Ceram. Int. **39**, 2283–2292 (2013).
[30] J. Cheng, J. Wang, X. Wang, and H. Wang, Ceram. Int. **43**, 7159–7165 (2017).
[31] D. Yuan, Z. Gao, Z. Jia, J. Shu, Y. Li, and X. Tao, Opt. Mater. **42**, 435–440 (2015).
[32] Z. Xu, Y. Li, Z. Liu, and D. Wang, J. Alloy Compd. **391**, 202–205 (2005).
[33] G. Mohan Kumar, P. Ilanchezhiyan, Fu Xiao, C. Siva, A. Madhan Kumar, V. Yalishev, Sh. U. Yuldashev, and T. W. Kang, RSC Adv. **6**, 57941–57947 (2016).
[34] I. Villa, A. Vedda, M. Fasoli, R. Lorenzi, N. Kränzlin, F. Rechberger, G. Ilari, D. Primc, B. Hattendorf, F. J. Heiligtag, M. Niederberger, and A. Lauria, Chem. Mater. **28**, 3245–3253 (2016).
[35] C. S. McCamy, Color Res. Appl. **17**, 142–144 (1992).
[36] A. I. Ramos-Guerra, J. Guzmán-Mendoza, M. García-Hipólito, O. Alvarez-Fregoso, and C. Falcony, Ceram. Int. **41**, 11279–11286 (2015).
[37] T. Li, P. L. Li, Z. J. Wang, S. C. Xu, Q. Y. Bai, and Z. P. Yang, Dalton Trans. **44**: 16840 (2015).